© 2017. Published by The Company of Biologists Ltd | Development (2017) 144, 830-836 doi:10.1242/dev.144063

RESEARCH REPORT

The assembly of developing motor neurons depends on an interplay between spontaneous activity, type II cadherins and gap junctions

Karli Montague[1], Andrew S. Lowe[2], Ana Uzquiano[3], Athene Knüfer[2], Marc Astick[4], Stephen R. Price[5] and Sarah Guthrie[2,*,‡]

ABSTRACT

A core structural and functional motif of the vertebrate central nervous system is discrete clusters of neurons or 'nuclei'. Yet the developmental mechanisms underlying this fundamental mode of organisation are largely unknown. We have previously shown that the assembly of motor neurons into nuclei depends on cadherin-mediated adhesion. Here, we demonstrate that the emergence of mature topography among motor nuclei involves a novel interplay between spontaneous activity, cadherin expression and gap junction communication. We report that nuclei display spontaneous calcium transients, and that changes in the activity patterns coincide with the course of nucleogenesis. We also find that these activity patterns are disrupted by manipulating cadherin or gap junction expression. Furthermore, inhibition of activity disrupts nucleogenesis, suggesting that activity feeds back to maintain integrity among motor neurons within a nucleus. Our study suggests that a network of interactions between cadherins, gap junctions and spontaneous activity governs neuron assembly, presaging circuit formation.

KEY WORDS: Motor neurons, Cell adhesion, Cadherins, Spontaneous activity, Gap junctions, Brainstem, Chick

INTRODUCTION

A key organisational motif of the central nervous system is assemblies of neurons with similar synaptic inputs, axonal outputs and functions. Neurons may assemble in clusters, termed nuclei, or in laminar structures such as the cerebral cortex or the cerebellum. Neuronal nucleus formation (nucleogenesis) is required for the correct acquisition of afferent input (Sürmeli et al., 2011), implying that nuclei are a crucial feature of neuronal circuits. Whereas the development of laminar structures has been extensively studied, the question of how nuclei form is unresolved. Here, we demonstrate that cell adhesion and spontaneous activity (SA), in the form of observable calcium transients, converge to shape motor nuclei of the vertebrate brainstem (Fig. 1A).

During nucleogenesis, facial and abducens motor neurons originate from overlapping rostrocaudal domains in rhombomeres (r) 4-6, but migrate differentially to segregate into nuclei at respective lateral and medial locations (Fig. 1B) (Guthrie, 2007). We have previously shown that type II cadherins play a pivotal role in motor nucleogenesis (Astick et al., 2014; Price et al., 2002). Coinciding with the period of neuronal segregation [embryonic day (E) 4-7], type II cadherin expression becomes refined (E5-6), including a change from widespread expression of cadherin 20 (*Cad20*) to expression of different combinations of cadherins by specific nuclei (Astick et al., 2014). Perturbing cadherin expression disrupts the segregation of abducens and facial neurons, suggesting a role for cadherin-mediated adhesion in nucleogenesis.

We hypothesised that SA might collaborate with cadherins to regulate nucleogenesis, with an adjunct role played by gap junctions (Fig. 1A). Whereas spontaneous electrical activity is known to regulate the late maturation of neuronal circuits (Yamamoto and López-Bendito, 2012), its influence on early developmental events, and interaction with molecular mechanisms has been unclear (Benjumeda et al., 2013; Hanson et al., 2008; Spitzer, 2006). However, rhythmic SA, which occurs in the absence of synaptic input, has previously been recorded from the avian cranial motor nerves at early developmental stages, suggesting a plausible involvement in nucleogenesis (Fortin et al., 1994, 1995).

Using the genetically encoded calcium indicator *GCaMP6*, we have optically imaged spontaneous calcium transients in facial and abducens motor neuron populations in the chick brainstem. We find that they exhibit characteristic SA patterns at E5 and E6. Manipulation of cadherins or gap junction coupling disrupts coordinated SA during nucleogenesis, and pharmacological disruption of SA *in vivo* impairs nucleogenesis, demonstrating a functional role for activity. These findings suggest that a network of interactions between cadherins, gap junctions and SA regulates and stabilises the formation of neuronal assemblies during development.

RESULTS AND DISCUSSION

Developing brainstem motor neurons show characteristic activity patterns

We introduced the genetically encoded calcium indicator *GCaMP6* (Chen et al., 2013) into chick hindbrains at E2 by electroporation (Hammond et al., 2005), and imaged activity in 'open book' hindbrain preparations at E5-6. The identity of *GCaMP*-expressing facial and abducens motor neurons was confirmed using cell position, and retrograde labelling in confocal *z*-stacks (Fig. 1C). Single optical planes in the r4-6 region were imaged to obtain functional time series (2-5 Hz; 3-10 min). At E5, we observed that motor neurons within a nucleus exhibited calcium transients (Movie 1), and that such activity was correlated among motor neurons within, but not between, facial and abducens populations within the same preparation (Fig. 1D), indicating that these neuronal subpopulations have independent SA patterns.

We focussed on the facial nucleus for more detailed analyses. Traces of normalised fluorescence changes (ΔF/F) from single facial

[1]Wolfson Centre for Age-related Diseases, King's College London, Guy's Hospital Campus, London SE1 1UL, UK. [2]Department of Developmental Neurobiology, King's College London, Guy's Hospital Campus, London SE1 1UL, UK. [3]École de Neuroscience-Paris Île-de-France, ENP-DIM, 15 Rue de L'École de Médécine, Paris 75006, France. [4]Institut de Recherche Interdisciplinaire en Biologie Humaine et Moléculaire, Université de Bruxelles, Route de Lennik 808, Bruxelles B1070, Belgium. [5]Department of Cell and Developmental Biology, University College London, Gower Street, London WC1E 6BT, UK.
*Present address: School of Life Sciences, University of Sussex, Brighton, BN1 9QG, UK.

‡Author for correspondence (s.guthrie@sussex.ac.uk)

S.G., 0000-0002-8446-9150

Received 24 August 2016; Accepted 10 January 2017

Development (2017) 144, 830-836 doi:10.1242/dev.144063

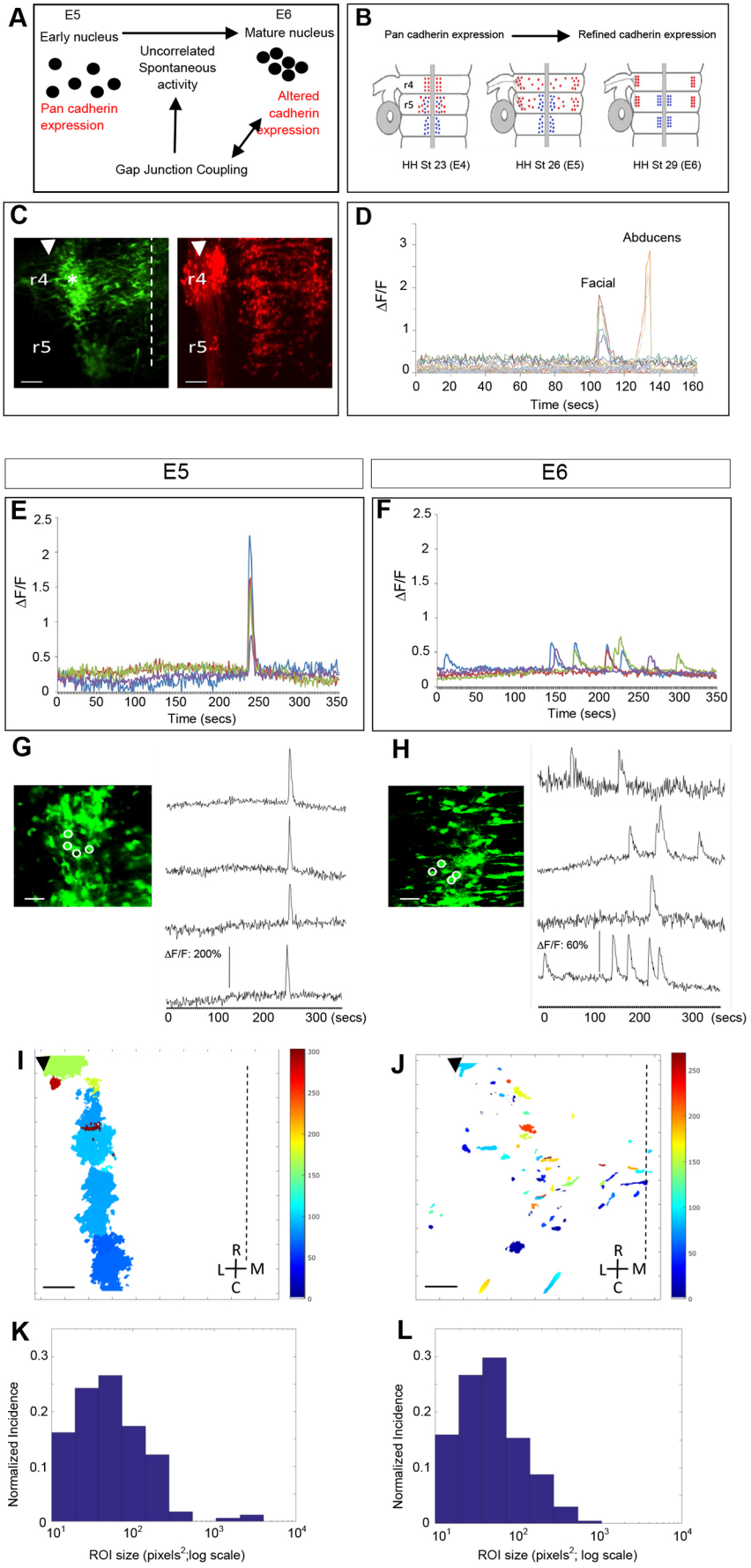

Fig. 1. Spontaneous activity of facial motor neurons shows different patterns at E5 and E6. (A) Schematic model of the role of nucleogenesis. (B) Schematic of rhombomeres (r) 4-6 of the chick hindbrain in 'open book' prep; the floor plate is positioned medially (grey bar), the facial nerve and otic vesicle (grey circle) are on the left. Facial and abducens motor neurons are indicated by red and blue circles, respectively. (C) *z*-stack confocal images of hindbrain with *GCaMP*-electroporated facial motor neurons (left) or retrogradely labelled with fluorescent rhodamine-dextrans (right). Dashed line indicates the floor plate; arrowhead indicates lateral edge of the neuroepithelium. The mature coalescing nucleus is shown by the asterisk. (D) E5 example time series showing normalised ΔF/F GCaMP fluorescence for individual facial and abducens neurons (n=3 preparations). (E,F) E5 (E) and E6 (F) example time series for ΔF/F of facial motor neurons [n=16 preparations (E) and n=17 preparations (F)]. (G,H) E5 (G) and E6 (H) examples of identified GCaMP-expressing facial motor neurons (left) with individual ΔF/F traces (right). Circles indicate the positions of cells from which traces were recorded. (I,J) E5 (I) and E6 (J) phase maps derived from individual time series showing active ROIs within the field of view of the facial motor nucleus. Colour represents time of activity peak (in seconds), with colder colours representing earlier events in the time series and warmer colours representing later events. Dashed line indicates floor plate; arrowhead indicates lateral edge of neuroepithelium. L-M, lateral-medial axis; R-C, rostral-caudal axis. (K,L) E5 (K) and E6 (L) plots of ROI size. The *x*-axis is the size of the region of interest (ROI in pixels^2; 100 pixels^2=25 μm^2) on a log scale; *y*-axis is the normalised incidence for each active ROI size, binned. Scale bars: 50 μm (C); 10 μm (G,H); 40 μm (I,J).

Development (2017) 144, 830-836 doi:10.1242/dev.144063

motor neurons at E5 showed calcium transients of duration 4-7 s that were temporally correlated (Fig. 1E,G). Calculation of the Pearson correlation coefficient for activity in each cell showed that all activity traces were significantly correlated between cells (P<0.05 for all possible pairings). These transients occurred at low frequency, with an average of one or two active regions of interest (ROIs; groups of cells showing coordinated activity) in a typical 5 min period (Fig. 1E; Fig. 2G). The range varied from one to seven per time series, with a wide variation in size (15-160 μm^2). The location and temporal distribution of ROIs was represented in phase maps that were created from the time series, representing the field of view that was imaged, in which colours were used to represent time (blue to red representing earlier to later events). Clusters of cells that showed activity were located in the more mature, lateral regions of the nucleus (Fig. 1I; Fig. 1C, asterisk) and not in medial regions containing younger, migrating motor neurons. The larger ROI sizes observed in Fig. 1I reflect the aggregation of many neighbouring cells with coherent activity, as can be seen by the quantitation of ROI size (Fig. 1K).

We found that facial motor neuron activity patterns changed at E6 (Movie 2; Fig. 1F,H). Calcium transients occurred at much higher frequency (six or seven in a 5 min period; P<0.01), but had smaller amplitude (P<0.05) (Fig. 2G,H). Activity was spread across a wider area of the nucleus (Fig. 1J), with ROIs that were significantly smaller on average than at E5 (Fig. 1L; P<0.05). Activity patterns are therefore different at E5 and E6, switching from infrequent, large coherent events involving neighbouring cells to numerous, smaller events. The correlation of activity observed within nuclei at E5 was also lost by E6, with only 34% of activity events significantly correlated (Pearson's correlation coefficient, P<0.05), coinciding with the timescale of coalescence of facial motor neurons to form a nucleus.

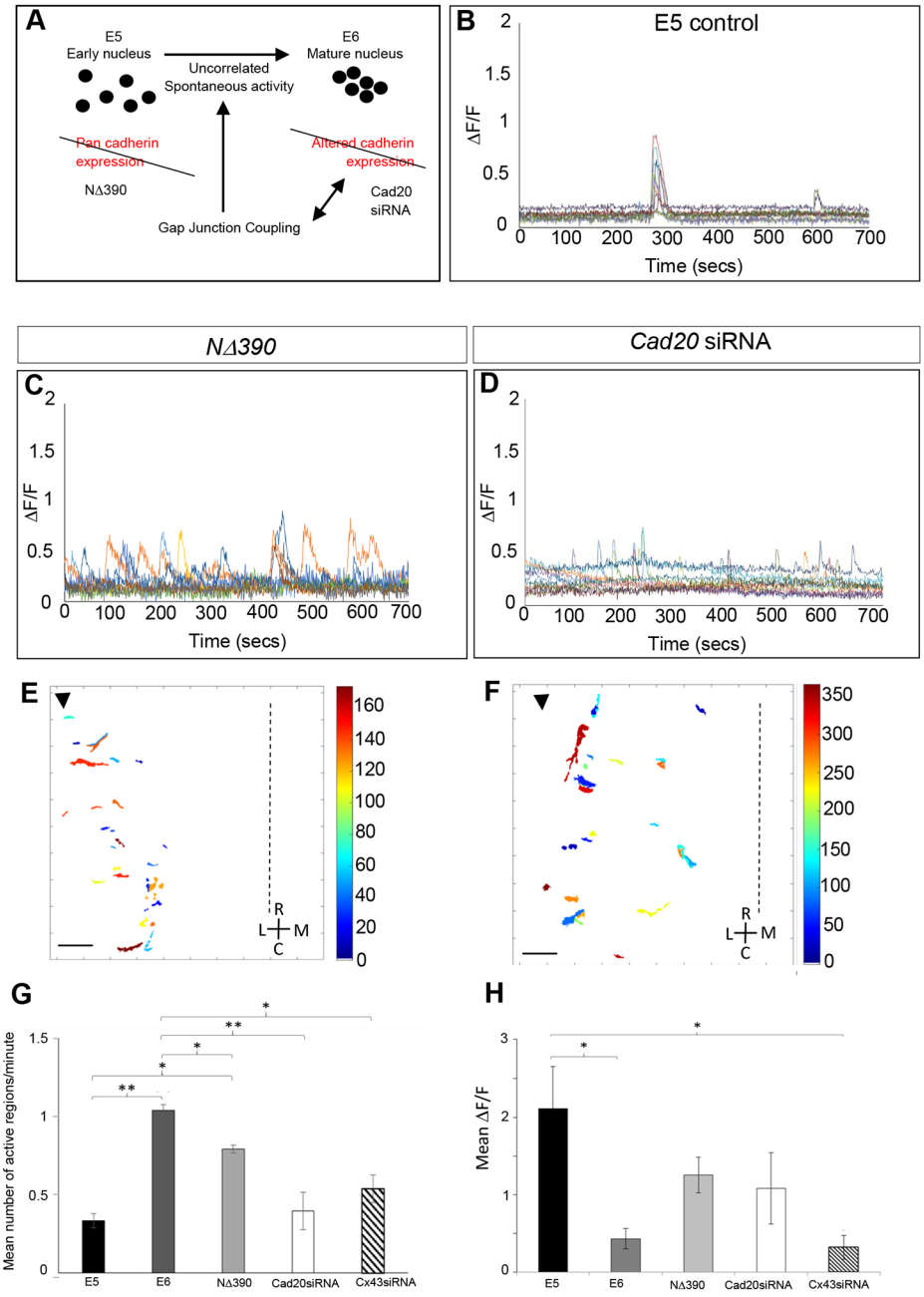

Fig. 2. Perturbing cadherin-dependent interactions disrupts motor neuron spontaneous activity. (A) Schematic model of perturbation of cadherin-dependent interactions. (B-D) E5 example time series for ΔF/F of facial motor neurons (GCaMP control, *NΔ390*/GCaMP, *Cad20* siRNA/GCaMP as labelled). Datasets are n=11 for *NΔ390* and n=4 for *Cad20* siRNA. (E,F) *NΔ390* (E) and *Cad20* (F) siRNA-electroporated hindbrain example phase maps, as in Fig. 1. Scale bars: 40 μm. (G) Frequency histogram showing mean number of bursts per minute for individual neurons. Compared with E5 controls, the frequency for E6 controls and *NΔ390* is significantly higher (**P<0.01 and *P<0.05, respectively). Compared with E6 controls, the frequency for *NΔ390*, *Cad20* siRNA and *Cx43* siRNA was significantly lower (*P<0.05, **P<0.01 and *P<0.05, respectively). (H) Histogram showing ΔF/F amplitude under conditions as labelled. Amplitude is significantly lower for E6 and for *Cx43* siRNA than for E5 (*P<0.05). Datasets for G and H are: E5 n=256 cells, E6 n=271 cells, *NΔ390* n=150 cells, *Cad20* siRNA n=43 cells, *Cx43* siRNA n=56 cells.

Development (2017) 144, 830-836 doi:10.1242/dev.144063

Pharmacological characterisation by bath-applying drugs and imaging GCaMP activity revealed that the activity depended on T type calcium channels at E5 (Fig. S1A,G), and on N and L type channels and endoplasmic reticulum-mediated calcium release at E6 (Fig. S1B,H-J). Spontaneous activity was insensitive to the sodium channel blocker tetrodotoxin (TTX) at E5 and E6 (Fig. S1D,E), but TTX abolished activity at E7 (Fig. S1F). These changes suggest that SA has a switch in calcium channel dependence between E5 and E6, with activity becoming synaptically driven from E7.

Manipulation of cadherin or connexins disrupts spontaneous activity patterns at E5

In view of the cadherin dependence of nucleogenesis in the hindbrain (Astick et al., 2014), we tested the idea that cadherin expression and SA are linked (Fig. 2A). We analysed SA patterns following disruption of cadherin signalling using a dominant-negative cadherin construct, *NΔ390* (Astick et al., 2014; Kintner, 1992), or an siRNA construct, which downregulates chicken *Cad20* (Fig. S2A,B). GCaMP imaging at E5 showed that, in both cases, there was a disruption of the typical SA patterns (Fig. 2B-D,G). The percentage of total events that were correlated fell to 42% for *NΔ390* and 11% for *Cad20* siRNA ($P<0.05$). For the *NΔ390* embryos, the frequency of transients were significantly increased ($P<0.05$) and the amplitude of transients was decreased relative to controls but not significantly (Fig. 2G,H). For the *Cad20* siRNA, the frequency was increased and the amplitude was reduced but neither change was significant (Fig. 2G,H). Phase maps showed ROIs to be more scattered and significantly smaller than in controls (Fig. 2E,F; Fig. S3B,C; $P<0.001$ and $P<0.01$ for *NΔ390* and *Cad20* siRNA, respectively). These data suggest that the global or specific de-regulation of cadherins disrupts SA patterns at E5.

In some contexts, SA events depend on gap junction coupling (Leybaert and Sanderson, 2012), and the gap junction protein connexin 43 (Cx43) has been linked to cadherin expression (Mendoza-Naranjo et al., 2012; Wei et al., 2005). In order to investigate a putative gap junction involvement, we first confirmed Cx43 expression by facial motor neurons using retrograde labelling and immunohistochemistry (Fig. 3A). To test the influence of gap junctions on SA (Fig. 3B), *Cx43* was knocked down using an siRNA (Fig. S2C,D) and SA was assessed at E5 as above. Activity patterns were strongly disrupted with an increase in frequency and a decrease in correlation, with only 23% of events correlated (Fig. 3C,D; Fig. 2G). The amplitude of transients was significantly reduced relative to E5 ($P<0.05$) and was more similar to E6 controls (Fig. 2H). Phase maps showed regions of SA to be more dispersed, with smaller ROIs (Fig. 3F; Fig. S3D). This suggests that facial motor neuron SA patterns are mediated by Cx43-containing gap junctions.

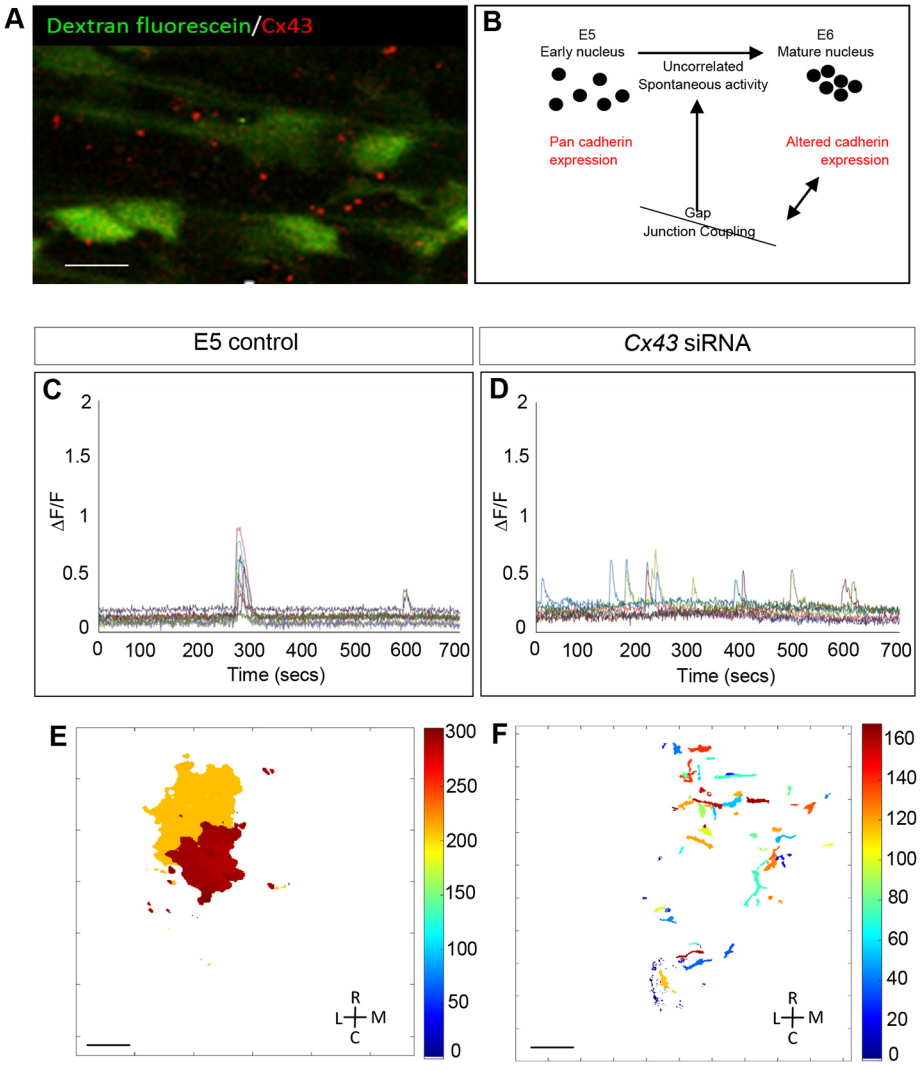

Fig. 3. Perturbing gap junction-dependent interactions disrupts motor neuron spontaneous activity. (A) Single confocal section showing retrogradely labelled facial motor neurons (green) and whole-mount immunofluorescence for the gap junction protein Cx43 (red). (B) Schematic model of perturbation of gap junction-dependent interactions. (C,D) E5 example time series for ΔF/F of facial motor neurons for GCaMP control (C) and *Cx43* siRNA/GCaMP (D). $n=4$ preparations. (E,F) E5 control (E) and *Cx43* siRNA-electroporated (F) hindbrain example phase maps, labelled as in Fig. 1. Scale bars: 7 µm (A); 35 µm (E,F).

Development (2017) 144, 830-836 doi:10.1242/dev.144063

Overall, cadherin and connexin manipulations produced activity patterns with qualitative and quantitative features that more closely resembled E6 than E5 controls.

Type II cadherins and Cx43 reciprocally regulate one another

We investigated a possible interplay between type II cadherins and Cx43 in NIH-3T3 cells, which express type II cadherins including *Cad11* (also known as *Cdh11*) (Takagi et al., 2012), which is expressed by both facial and abducens neurons (Astick et al., 2014). We confirmed expression of *Cad11* and *Cx43* (also known as *Gja1*) at cell junctions, and quantified the density of puncta in untransfected and GFP-transfected control cells using immunohistochemistry (Fig. S4A,D). Downregulation or upregulation of cadherins using the *NΔ390* dominant-negative construct or *Cad20* full-length construct led to a significant decrease and increase, respectively, in the density of Cx43 puncta at cell junctions relative to controls (Fig. S4A-C; $P<0.01$; $P<0.001$). Conversely, siRNA-mediated knockdown of *Cx43* expression significantly reduced Cad11

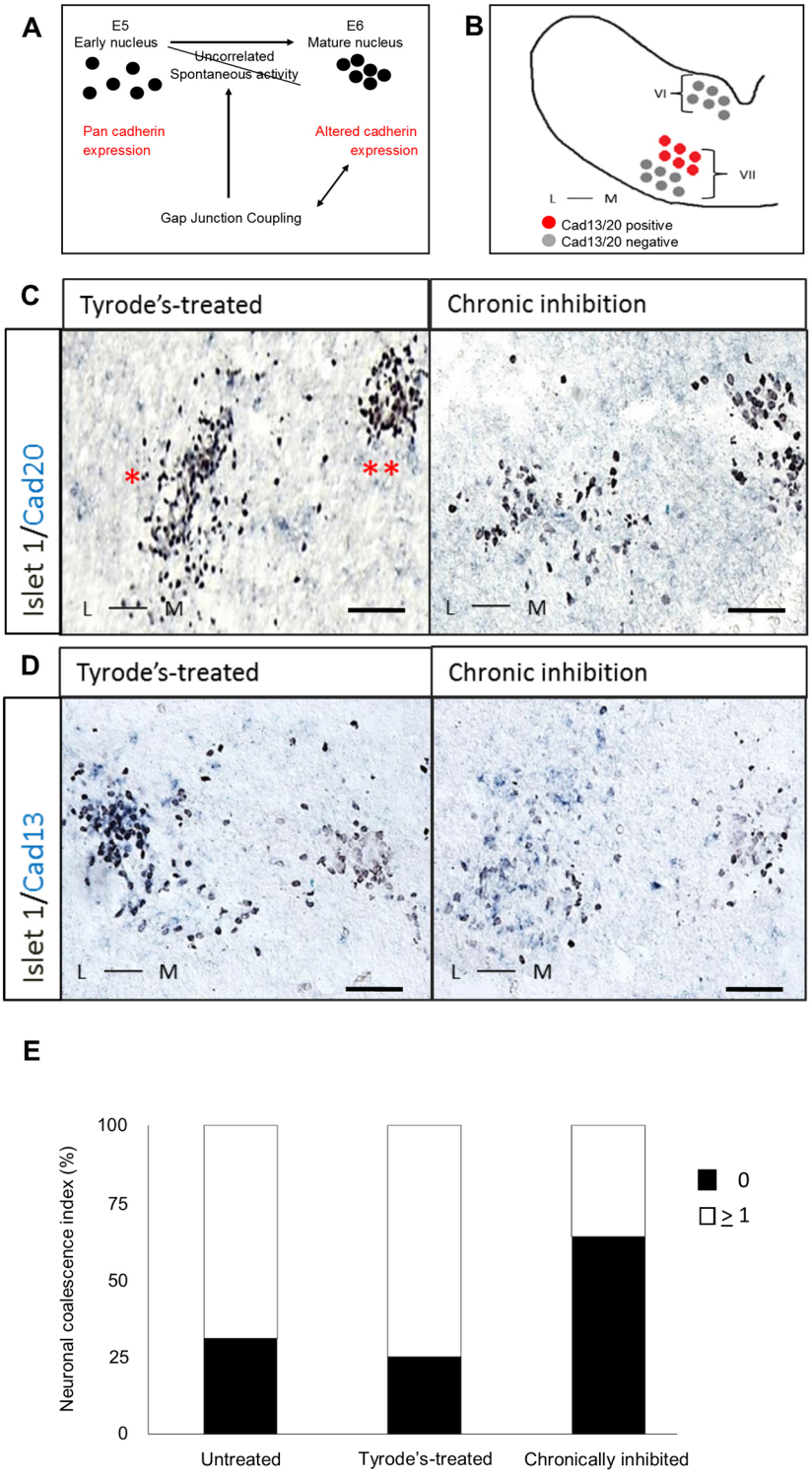

Fig. 4. The effect of chronic activity inhibition on nucleogenesis and cadherin expression. (A) Schematic model of perturbation of spontaneous activity. (B) Schematic of an E6 transverse hindbrain section showing the mediolateral (L-M) location of facial (VII) and abducens (VI) motor neurons, and pattern of *Cad13*/*Cad20* expression. (C,D) E6 transverse hindbrain sections immunostained for the motor neuron-specific marker Islet 1 (dark brown), showing the facial (single asterisk) and the abducens (double asterisk) motor nuclei. *In situ* hybridisation for either *Cad20* (C) or *Cad13* (D) was carried out on the same sections. Left: control, vehicle-treated embryos (Tyrode's solution); right: calcium channel blocker-treated embryos. Scale bars: 10 µm. (E) Quantification of facial motor nucleus coalescence in embryos as labelled. The proportion of facial motor neurons with no juxtaposing motor neurons increases significantly ($P<0.01$) following activity inhibition ($n=3$ experiments, 8-10 embryos per experiment).

Development (2017) 144, 830-836 doi:10.1242/dev.144063

immunoreactivity at cell junctions relative to controls (Fig. S4D,E; $P<0.001$). These results therefore suggest that there is a reciprocal regulation of type II cadherins and Cx43 *in vitro*.

Inhibition of spontaneous activity perturbs nucleogenesis *in vivo*

The results of these *in vivo* and *in vitro* experiments suggest that a dynamic interplay between cadherins and connexins regulates SA. We then asked whether, conversely, SA might regulate the topography of the nascent motor nucleus, and cadherin expression. SA was inhibited by applying a cocktail of calcium channel inhibitors found to block activity at E5-6 to chick embryos *in ovo* for 24 h from E5 to E6 (Fig. 4A). At E6, the distribution of facial and abducens motor neurons was analysed by immunohistochemistry and the expression levels of two relevant cadherins, *Cad20* and *Cad13*, were analysed by *in situ* hybridisation (Fig. 4B) (Astick et al., 2014). A normal segregation of facial and abducens neuronal clusters and of cadherin expression was observed in vehicle-treated embryos (Fig. 4C,D). Activity blockade resulted in neuronal disaggregation, as quantified using a coalescence index for neuronal clustering (Fig. 4C-E; $P<0.01$), suggesting that SA might itself stabilise topography within the facial nucleus. Whereas *Cad20* levels were normal in SA-inhibited embryos, *Cad13* expression appeared to be reduced (Fig. 4C,D). We therefore propose the presence of a feedback loop that allows SA to regulate nucleogenesis.

Conclusions and implications of our findings

This study reports a novel interplay between SA and cadherin-mediated adhesion in neuronal nucleus formation. Cadherins, gap junctions and SA form a regulatory network that underpins nucleogenesis. We propose that the initial expression of cadherins among motor neurons drives their migration and segregation into a loose, immature nucleus, whereas the onset of correlated activity regulates nuclear maturation and the emergence of functional properties. Once the nucleus has matured and cadherin expression is refined, the pattern of SA changes from spreading waves to small, dispersed cell groups.

Perturbation experiments suggested that the early (E5) phase of ensemble activity in particular is cadherin and connexin dependent. Manipulations of cadherins did not significantly decrease the amplitude of calcium transients, suggesting that the activity of individual motor neurons was largely unchanged. By contrast, *Cx43* knockdown produced a significant reduction in amplitude, implying an effect on the ability of individual neurons to generate SA.

Reciprocal regulation between Cx43 and type I cadherins is well-established though a direct interaction has not been shown (Mendoza-Naranjo et al., 2012; Wei et al., 2005). Our *in vitro* data suggest a similar reciprocal interaction between Cx43 and type II cadherins; however, *in vivo* experiments failed to detect a significant change in Cx43 localisation following siRNA-mediated *Cad20* downregulation (data not shown). The mechanism by which inhibition of SA results in the disruption of nucleogenesis could be via an effect on cadherin expression.

Our observations show similarities with the correlated SA that has been reported in the developing retina (Feller et al., 1996; Graeber et al., 2013), and in chick and zebrafish spinal motor neurons (Law et al., 2014; Plazas et al., 2013; Wang et al., 2009), where in one case activity was thought to be regulated by recurrent synaptic excitation.

Whereas previous studies focussed on the relationship between activity and axon guidance or topographic mapping, here we focus specifically on the relationship between SA and molecules at the level of motor neuron cell bodies. Our findings highlight the collaboration of molecular mechanisms of cell adhesion and activity in organising neuronal assemblies. Cadherin/catenin signalling has also been shown to pattern spinal motor neuron cell bodies (Demireva et al., 2011). We can speculate that events during nucleogenesis are autonomous to neuronal soma; indeed the caudal migration of mouse facial motor neurons occurs in hindbrain explants without peripheral axons (Vivancos et al., 2009).

The activity we describe might also regulate neuronal maturation and the acquisition of afferent input, which may include descending input from early longitudinal tracts and the vestibular and raphe spinal systems (Gilland and Baker, 2005; Hughes et al., 2009). The link between motor nucleogenesis and brainstem neuronal circuit formation remains to be characterised.

MATERIALS AND METHODS

Avian embryos

Fertilised Brown Bovan Gold Hen's eggs (Henry Stewart & Co, UK) were incubated at 38°C to E2-7 and staged according to Hamburger and Hamilton (1992).

In ovo electroporation

Expression of constructs was achieved by *in ovo* electroporation at E2 as described (Ferrario et al., 2012). Retrograde labelling of the facial nerve was carried out as previously described (Simon and Lumsden, 1993). See supplementary Materials and Methods for further details.

GCaMP imaging

For live imaging of *GCaMP*-electroporated hindbrains, avian embryos were harvested at 37°C, in oxygenated Tyrode's solution, and pinned ventral-side up in a Sylgard dish. Mesenchyme was removed from the hindbrain, and movies were acquired on an Eclipse Ni-E Upright CSU-X1 Spinning Disc confocal microscope equipped with an Andor iXon 3 EM-CCD camera and NIS elements AR software. All other images or *z*-stacks were acquired using a Zeiss Upright Fluorescence microscope with QImaging CCD digital camera and Volocity software, or an upright Nikon confocal microscope with EZ-C1 software.

Image processing

For single motor neuron traces, regions of interest were created around identified facial and abducens motor neurons. Normalised fluorescence changes were calculated as $\Delta F/F=(F-F0)/(F0)$, where F was the background-corrected average fluorescence signal within the ROI, and F0 was the background-corrected average intensity at the resting level using Fiji software. Movies were further processed using image registration to reduce the drift. Subsequently, a voxel-wise estimation of $\Delta F/F$ was calculated based on lower percentile of baseline signal, and then an estimation of skewness was calculated to derive regions of activity quantitatively. Phase maps were also constructed for each time series. See supplementary Materials and Methods for details of ROI analysis.

Pharmacological treatment during live imaging

GCaMP-electroporated chick embryos were dissected and hindbrains were imaged using a spinning disc confocal microscope as described. Embryos were equilibrated at 37°C in oxygenated Tyrode's solution for 30 min and pharmacological reagents were applied [0.5 µM TTX; 100 µM $NiCl_2$; 300 nM conotoxin; 10 µM nifedepine; 100 µM 2-aminoethoxydiphenyl borate (APB)]. Rhombomeres 4-6 of the hindbrain were then imaged for 10 min before the reagents were washed out with fresh oxygenated Tyrode's solution at 37°C, allowing activity to recover.

Inhibition of spontaneous activity

Eggs were windowed at E5 (HH stage 25) and either left untreated or treated with sterile Tyrode's solution or a solution containing 300 nM conotoxin (Tocris Bioscience), 10 µM nifedepine (Sigma), 100 µM $NiCl_2$ (Sigma) and

Development (2017) 144, 830-836 doi:10.1242/dev.144063

100 µM APB (Sigma). These reagents were infused into the egg every 4 h over 24 h and the egg then re-sealed. Embryos were fixed in 4% paraformaldehyde after 24 h, dehydrated in increasing concentrations of sucrose (up to 30%), snap-frozen, cryosectioned and processed for *in situ* hybridisation and immunohistochemistry (see supplementary Materials and Methods for details, including antibodies used).

NIH-3T3 cell culture

NIH-3T3 cells were grown in Dulbecco's Modified Eagle Medium/Nutrient Mixture F-12 (DMEM F12, Invitrogen) supplemented with 10% foetal bovine serum (FBS; Invitrogen) and 1% penicillin-streptomycin. Cultures were grown on glass coverslips in 24-well plates to 80% confluency. Lipofectamine LTX (Invitrogen) along with DNA plus reagent (Invitrogen) was used to transfect the cells with the cadherin (*NΔ390* and *Cad20*), and *Cx43* siRNA constructs. All constructs used were co-transfected with a GFP plasmid in order to assess transfection efficiency. See supplementary Materials and Methods for details of validation of siRNA constructs and NIH-3T3 cell immunocytochemistry.

CHO cell culture

Chinese hamster ovary (CHO) cells were grown in DMEM (Invitrogen) supplemented with 10% FBS. Cells were allowed to reach at least 80% confluency before being transfected with the chicken *Cad20* siRNA or chicken *Cx43* siRNA constructs. Transfection was carried out as described for NIH-3T3 cells. The CHO cells were left in culture for a further 48 h before being homogenised for western blots (see supplementary Materials and Methods for details).

Statistical analysis

The significance of differences in activity frequency, amplitude and ROI size between different manipulations and stages was tested using a paired Student's *t*-test. Correlation of activity was assessed using Pearson's correlation coefficient. All statistical tests were performed using SPSS.

Acknowledgements

We thank Uwe Drescher, Camilla Larsen and QueeLim Ch'ng for valuable advice and discussion. We thank Aine Rubikaite for validation of siRNA constructs, and Ana Casimiro De Almeida, Chiraag Thakrar and Pranetha Baskaran for technical assistance.

Competing interests

The authors declare no competing or financial interests.

Author contributions

S.G., K.M. and S.R.P. designed the research; K.M., A.U., A.K., M.A. and S.R.P. performed the research; K.M., A.S.L. and S.G. analysed data; S.G., K.M., A.S.L. and S.R.P. wrote the paper.

Funding

This work was funded generously by the Wellcome Trust. A.K. was funded by a Biotechnology and Biological Sciences Research Council PhD studentship. Deposited in PMC for release after 6 months.

Supplementary information

Supplementary information available online at
http://dev.biologists.org/lookup/doi/10.1242/dev.144063.supplemental

References

Astick, M., Tubby, K., Mubarak, W. M., Guthrie, S. and Price, S. R. (2014). Central topography of cranial motor nuclei controlled by differential cadherin expression. *Curr. Biol.* **24**, 2541-2547.

Benjumeda, I., Escalante, A., Law, C., Morales, D., Chauvin, G., Muca, G., Coca, Y., Marquez, J., Lopez-Bendito, G., Kania, A. et al. (2013). Uncoupling of EphA/ephrinA signaling and spontaneous activity in neural circuit wiring. *J. Neurosci.* **33**, 18208-18218.

Chen, T.-W., Wardill, T. J., Sun, Y., Pulver, S. R., Renninger, S. L., Baohan, A., Schreiter, E. R., Kerr, R. A., Orger, M. B., Jayaraman, V. et al. (2013). Ultrasensitive fluorescent proteins for imaging neuronal activity. *Nature* **499**, 295-300.

Demireva, E. Y., Shapiro, L. S., Jessell, T. M. and Zampieri, N. (2011). Motor neuron position and topographic order imposed by beta- and gamma-catenin activities. *Cell* **147**, 641-652.

Feller, M. B., Wellis, D. P., Stellwagen, D., Werblin, F. S. and Shatz, C. J. (1996). Requirement for cholinergic synaptic transmission in the propagation of spontaneous retinal waves. *Science* **272**, 1182-1187.

Ferrario, J. E., Baskaran, P., Clark, C., Hendry, A., Lerner, O., Hintze, M., Allen, J., Chilton, J. K. and Guthrie, S. (2012). Axon guidance in the developing ocular motor system and Duane retraction syndrome depends on Semaphorin signaling via alpha2-chimaerin. *Proc. Natl. Acad. Sci. USA* **109**, 14669-14674.

Fortin, G., Champagnat, J. and Lumsden, A. (1994). Onset and maturation of branchio-motor activities in the chick hindbrain. *Neuroreport* **5**, 1149-1152.

Fortin, G., Kato, F., Lumsden, A. and Champagnat, J. (1995). Rhythm generation in the segmented hindbrain of chick embryos. *J. Physiol.* **486**, 735-744.

Gilland, E. and Baker, R. (2005). Evolutionary patterns of cranial nerve efferent nuclei in vertebrates. *Brain Behav. Evol.* **66**, 234-254.

Graeber, C. P., Hunter, D. G. and Engle, E. C. (2013). The genetic basis of incomitant strabismus: consolidation of the current knowledge of the genetic foundations of disease. *Semin. Ophthalmol.* **28**, 427-437.

Guthrie, S. (2007). Patterning and axon guidance of cranial motor neurons. *Nat. Rev.* **8**, 859-871.

Hamburger, V. and Hamilton, H. L. (1992). A series of normal stages in the development of the chick embryo. 1951. *Dev. Dyn.* **195**, 231-272.

Hammond, R., Vivancos, V., Naeem, A., Chilton, J., Mambitisaeva, E., Andrews, W., Sundaresan, V. and Guthrie, S. (2005). Slit-mediated repulsion is a key regulator of motor axon pathfinding in the hindbrain. *Development* **132**, 4483-4495.

Hanson, M. G., Milner, L. D. and Landmesser, L. T. (2008). Spontaneous rhythmic activity in early chick spinal cord influences distinct motor axon pathfinding decisions. *Brain Res. Rev.* **57**, 77-85.

Hughes, S. M., Easton, C. R. and Bosma, M. M. (2009). Properties and mechanisms of spontaneous activity in the embryonic chick hindbrain. *Dev. Neurobiol.* **69**, 477-490.

Kintner, C. (1992). Regulation of embryonic cell adhesion by the cadherin cytoplasmic domain. *Cell* **69**, 225-236.

Law, C., Paquet, M. and Kania, A. (2014). Emergence of motor circuit activity. *PLoS ONE* **9**, e93836.

Leybaert, L. and Sanderson, M. J. (2012). Intercellular Ca(2+) waves: mechanisms and function. *Physiol. Rev.* **92**, 1359-1392.

Mendoza-Naranjo, A., Cormie, P., Serrano, A. E., Hu, R., O'Neill, S., Wang, C. M., Thrasivoulou, C., Power, K. T., White, A., Serena, T. et al. (2012). Targeting Cx43 and N-cadherin, which are abnormally upregulated in venous leg ulcers, influences migration, adhesion and activation of Rho GTPases. *PLoS ONE* **7**, e37374.

Plazas, P. V., Nicol, X. and Spitzer, N. C. (2013). Activity-dependent competition regulates motor neuron axon pathfinding via PlexinA3. *Proc. Natl. Acad. Sci. USA* **110**, 1524-1529.

Price, S. R., De Marco Garcia, N. V., Ranscht, B. and Jessell, T. M. (2002). Regulation of motor neuron pool sorting by differential expression of type II cadherins. *Cell* **109**, 205-216.

Simon, H. and Lumsden, A. (1993). Rhombomere-specific origin of the contralateral vestibulo-acoustic efferent neurons and their migration across the embryonic midline. *Neuron* **11**, 209-220.

Spitzer, N. C. (2006). Electrical activity in early neuronal development. *Nature* **444**, 707-712.

Sürmeli, G., Akay, T., Ippolito, G. C., Tucker, P. W. and Jessell, T. M. (2011). Patterns of spinal sensory-motor connectivity prescribed by a dorsoventral positional template. *Cell* **147**, 653-665.

Takagi, R., Yamato, M., Kushida, A., Nishida, K. and Okano, T. (2012). Profiling of extracellular matrix and cadherin family gene expression in mouse feeder layer cells: type VI collagen is a candidate molecule inducing the colony formation of epithelial cells. *Tissue Eng. A* **18**, 2539-2548.

Vivancos, V., Chen, P., Spassky, N., Qian, D., Dabdoub, A., Kelley, M., Studer, M. and Guthrie, S. (2009). Wnt activity guides facial branchiomotor neuron migration, and involves the PCP pathway and JNK and ROCK kinases. *Neural Dev.* **4**, 7.

Wang, S., Polo-Parada, L. and Landmesser, L. T. (2009). Characterization of rhythmic Ca2+ transients in early embryonic chick motoneurons: Ca2+ sources and effects of altered activation of transmitter receptors. *J. Neurosci.* **29**, 15232-15244.

Wei, C.-J., Francis, R., Xu, X. and Lo, C. W. (2005). Connexin43 associated with an N-cadherin-containing multiprotein complex is required for gap junction formation in NIH3T3 cells. *J. Biol. Chem.* **280**, 19925-19936.

Yamamoto, N. and López-Bendito, G. (2012). Shaping brain connections through spontaneous neural activity. *Eur. J. Neurosci.* **35**, 1595-1604.

Montague et al. Supplementary Information

Supplementary Figures

Figure S1

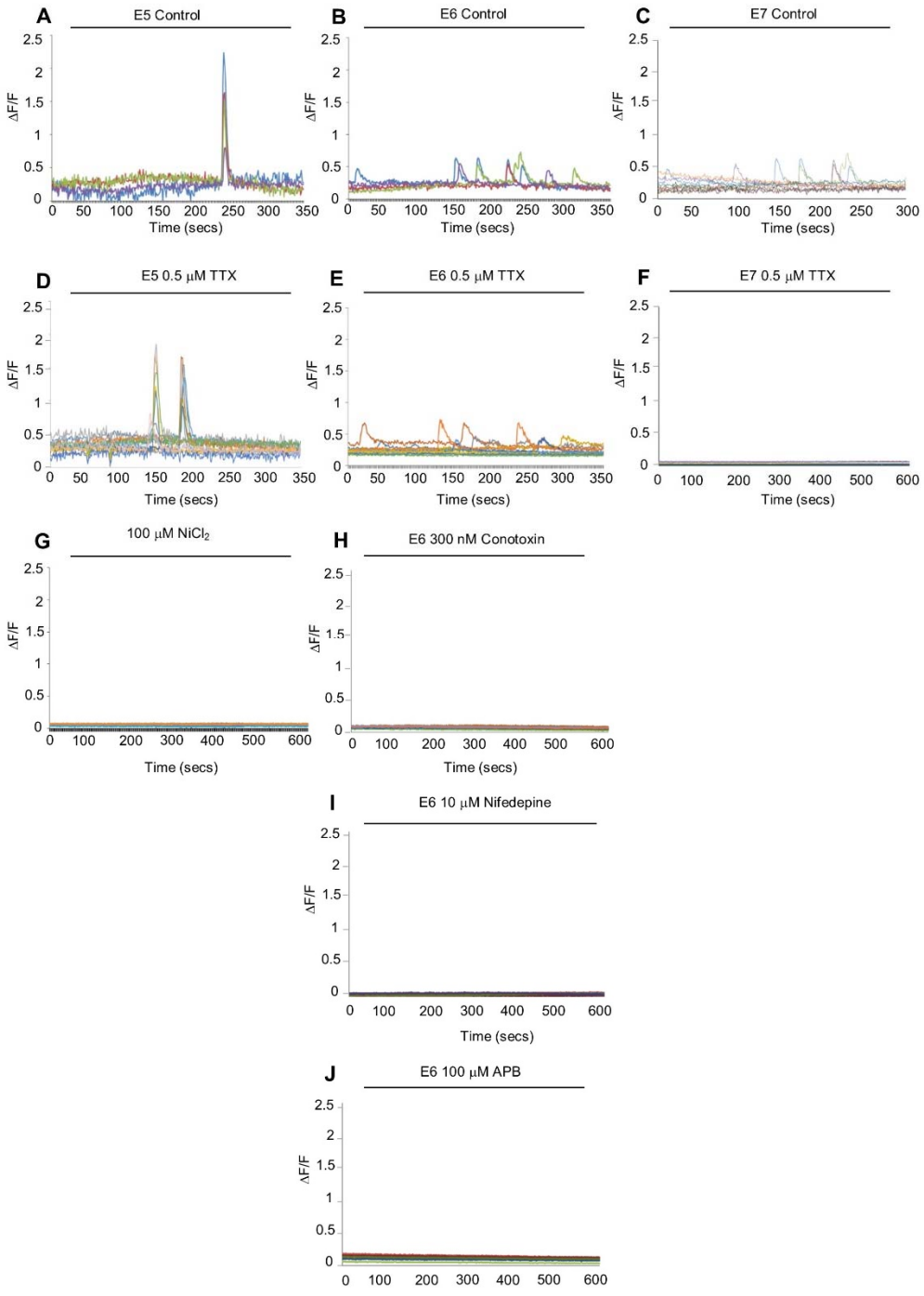

Figure S1: Pharmacological characterisation of spontaneous activity (SA) in facial motor neurons

Pharmacological characterisation of SA in facial motor neurons at E5 (A), (D), (G), E6 (B), (E), (H), (I), (J) and E7 (C), (F) showing typical examples of ΔF/F neuron traces for individual time series of duration 350 – 600 secs. Treatments with tetrodotoxin (TTX) and calcium channel blockers; T-type calcium channel blocker $NiCl_2$, N- and L-type voltage-gated calcium channel blockers Conotoxin and Nifedepine, respectively, and 2-Aminoethoxydiphenyl Borate (2-APB), which block calcium release from the endoplasmic reticulum, as labelled. For all treatments n = 3 preparations.

Figure S2

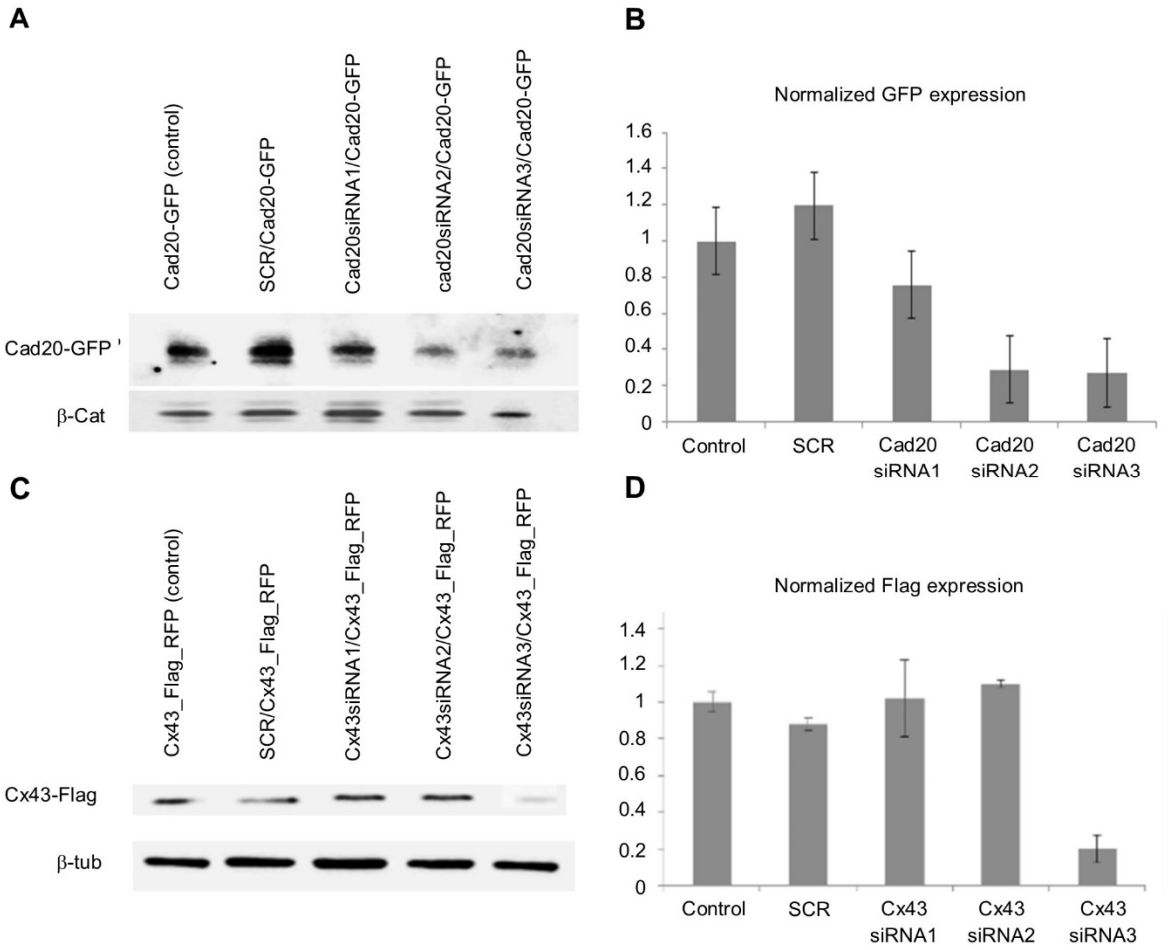

Figure S2: siRNA construct validation

siRNA constructs, designed to downregulate chick *cad20* (A) or *Cx43* (C) were tested using western blot analysis of CHO cells co-transfected with full length GFP-tagged *cad20* or Flag-tagged *Cx43* and the corresponding siRNA. In all cases the effect of the siRNA construct on target protein expression was compared to expression in untransfected and scrambled siRNA-transfected cultures. Blot loading controls were β-catenin and β-tubulin, as shown. Band intensities were measured densitometrically and compared with appropriate loading controls to derive a normalized expression level, where control (untransfected cells) is 1. The most efficient construct (siRNA3 in each case) was used for all experiments in vivo. N = 3 for all constructs.

Figure S3

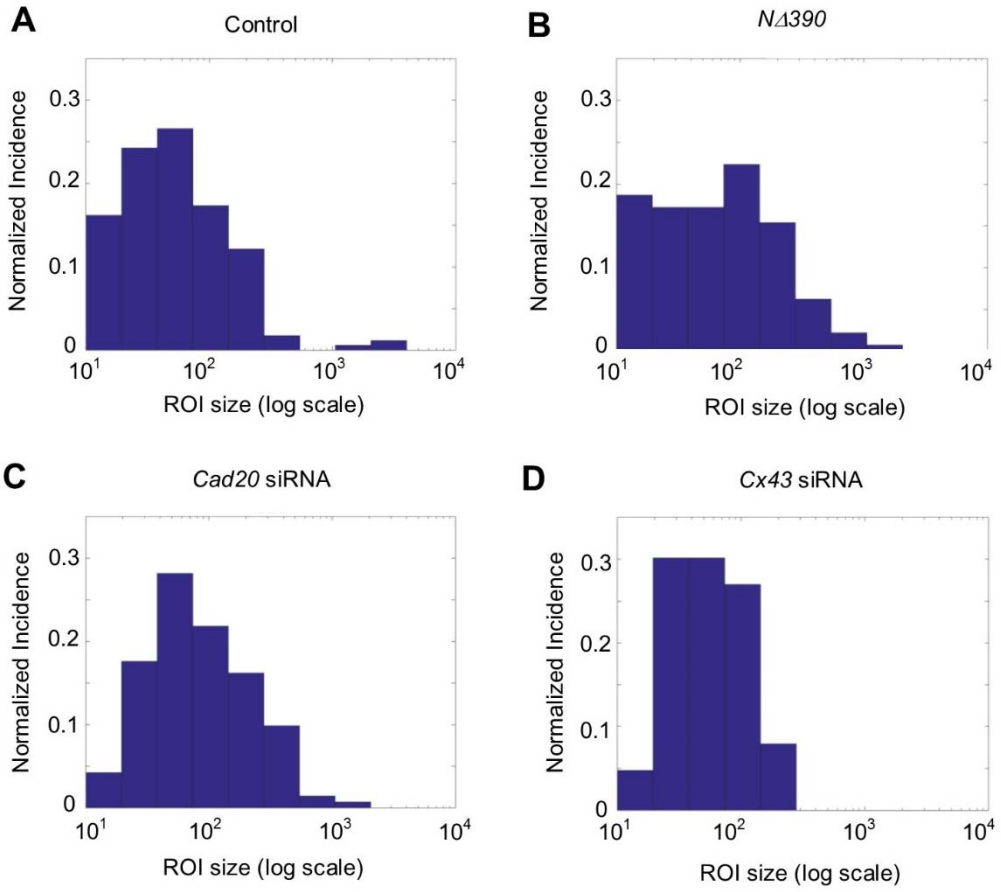

Figure S3: Comparison of ROI size in E5 controls, cadherin and gap junction manipulated-embryos

Histograms (as labelled) show binned ROI sizes on a log scale (X axis; pixels^2) versus normalized incidence on Y axis. Manipulated embryos show a trend towards smaller ROI size relative to controls.

Figure S4

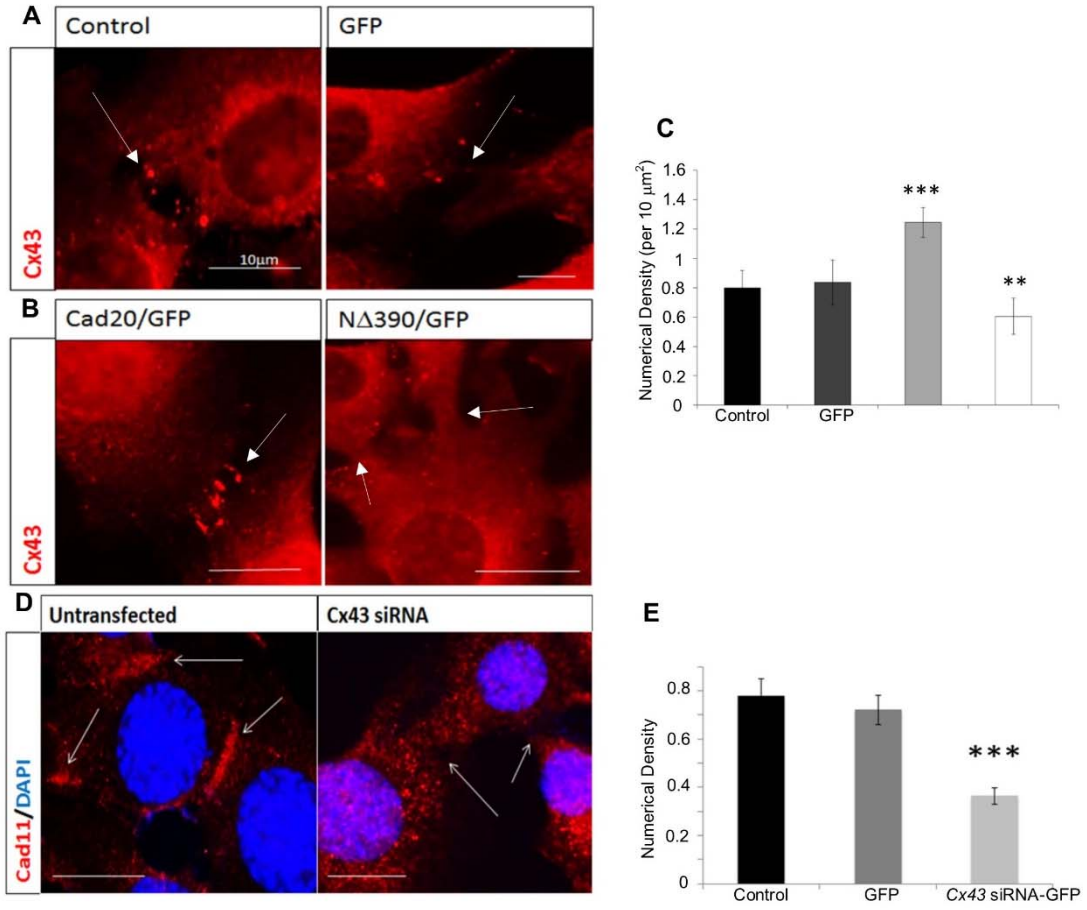

Figure S4: Reciprocal interaction between type II cadherins and Cx43 in vitro
(A) Untransfected and GFP-transfected NIH-3T3 cell cultures immunostained for Cx43 (red), showing puncta at cell-cell junctions (arrows). (B) Full-length *cad20*- and dominant negative *NΔ390*-transfected NIH3T3 cells immunostained for Cx43. Scale bar – 10 μm. (C) Quantitation of puncta density per unit area under different conditions, showing that *Cad20* significantly increased expression (***p < 0.001 relative to untransfected), whereas *NΔ390* transfection significantly decreased expression (**p < 0.01: relative to untransfected). (D) Untransfected and Cx43-siRNA-transfected NIH-3T3 cells immunostained for cad11, (red) and DAPI (blue). Quantitation of puncta density as above, showing that Cx43 down-regulation decreased puncta density significantly (***p < 0.001 relative to untransfected). In all experiments n = 3 cultures.

Supplementary Materials and Methods

In Ovo Electroporation

Briefly, approximately 0.1 µl of DNA construct (2 µg/µl in H_2O with 0.1% Fast Green (Sigma)) was pressure-injected into the lumen of the caudal hindbrain of E2 embryos. Electrodes were placed with the anode beneath and the cathode above the hindbrain and five 20 V, 50 ms pulses were applied using a dual-pulse isolated stimulator (Intracel, UK). Embryos were regularly hydrated with Tyrode's solution (137 mM NaCl, 5.6 mM D-Glucose, 2.7 mM KCl, 1 mM $MgCl_2.6H_2O$, 1.8 mM $CaCl_2.2H_2O$, 0.44 mM $NaH_2PO4.2H_2O$, 11.4 mM NaHCO3 and 1 in 50 penicillin-streptomycin solution; pH 7.4). Embryos were imaged at E5-7.

ROI analysis

For ROI analysis, confocal time series images were median and Gaussian filtered and changes in signal (ΔF and ΔF/F) were determined. In-house scripts delineated ROI automatically based on whether voxels exhibited skewed deviations in space and time. The ROI segmentation was based on the degree of skewness of the noise distribution rather than a threshold based on a peak signal. This is performed on a pixel-wise basis and in data that was subject to minimal blurring as all imaging was performed with a closed aperture, and there was no image filter applied post-processing. Given the large range of ROI areas, histograms using logarithmic spaced bins were calculated. Area-normalised bar charts enabled direct comparisons of distributions in ROI size across groups.

Validation of siRNA constructs

To evaluate the efficiency of knockdown by *cad20* and *Cx43* siRNAs, we used a GFP-tagged chicken *cad20*, or a Flag-tagged chicken *Cx43* expression construct. Chinese Hamster Ovary (CHO) cells were transfected with these constructs and corresponding siRNAs, including the empty vector and scrambled siRNA as controls. After 48 hrs in culture, Western blots were carried out and silencing was assessed by densitometry relative to controls (Fig. S3). The most efficient downregulation was 73% for *cad20* siRNA 3 (sequence GCAGCGCAAGAGTTGTGTAC (sense)) and 80% for *Cx43* siRNA 3 (sequence GTACTCAACAGCCTGGTTGT (sense)). These siRNAs were used in all subsequent experiments.

Antibodies

All primary and secondary antibodies were diluted in a blocking solution suitable for the protocol. *Primary antibodies*: chicken polyclonal anti-GFP, 1:1000 (Abcam); rabbit polyclonal GFP, 1:1000 (Abcam); rabbit polyclonal anti-OB cadherin (Cad11), 1:800 (Abcam); mouse monoclonal 4D5 anti-Islet-1 (Developmental Studies Hybridoma Bank); rabbit polyclonal anti-connexin 43 (Cx43), 1:1000 (Abcam), mouse monoclonal anti-FLAG, 1:1000 (Sigma); rabbit polyclonal anti-beta tubulin, 1:1000 (Abcam); rabbit polyclonal anti-beta catenin, 1:1000 (Abcam).

Secondary antibodies: Alexa-488 anti-rabbit; Alexa-488 anti-chicken; Alexa-488 anti-mouse; Alexa-568 anti-rabbit; Alexa-568 anti-mouse; Alexa-633 anti-mouse (all raised in goat and used at 1:1000, Invitrogen). Anti-rabbit HRP, 1:5000 (Thermo Scientific), anti-mouse HRP, 1:5000 (Sigma Aldrich).

Immunohistochemistry and in situ hybridisation

Immunohistochemistry on whole-mounts was performed as previously described (Ferrario et al., 2012). Dual in situ hybridisation with immunohistochemistry was performed as previously described (Astick et al., 2014), using digoxigenin (DIG; Sigma Aldrich, UK)-labelled anti-sense cRNA probes, but replacing the proteinase K treatment with a 30 min incubation with 0.1% PBST (pH7.4). Development of the RNA in situ hybridisation was followed by incubation with the anti-Islet-1 primary antibody for 16 hrs at 4^{o}C, secondary HRP-conjugated goat anti-mouse antibodies for 2 hrs were then applied and ImPact DAB substrate reagent (Vector labs) was used, following the manufacturer's instructions.

The nuclear coalescence index was calculated as previously described in order to determine the clustering of motor neurons within a nucleus (Astick et al., 2014). In short, individual neurons of the same type were chosen and the number of neurons surrounding it (within 1 micron) that were of the same identity counted. Neurons in the zero bin are thus separated from their neighbours. Neurons in the remaining bin had at least one neighbour adjacent and were deemed to be within the nucleus proper.

NIH-3T3 cell immunocytochemistry

For immunocytochemistry, cells were fixed in 4% PFA (15 mins), permeabilised in 0.1% PBST (5 mins), and blocked in 1% BSA-PBST for 1 hr, all at room temp. Cells were incubated in primary antibody for 16 hrs at 4^{o}C, washed in 0.1% PBST (3 x 5 mins), and incubated in secondary antibody for 2 hrs at room temperature, before washing and mounting on glass slides coated with FluorSave™ Reagent (Millipore). Puncta density was quantitated using Fiji software.

Western blotting

CHO cells were homogenized on ice in lysis buffer (Tris-HCl, 20 mM pH 7.5, 10 mM NaF, 150 mM NaCl, 1% Nonidet P-40, 1 mM phenyl-methylsulfonyl fluoride fluoride, 1 mM Na3VO4,10 mg/mL leupeptin and trypsin inhibitor) with complete mini cocktail protease inhibitor (Roche). Samples were agitated for 30 mins at 4^{o}C before being centrifuged at 16,000 rpm for 20 minutes at 4˚C. The protein concentration of the supernatant was determined using the NanoDrop spectrometer (Thermo Fisher Scientific). Equal protein concentrations per sample (20 mg of protein) were added to an equal volume of 1x Laemmli sample buffer, boiled for 5 minutes at 95^{o}C, and separated in a 15% SDS-PAGE gel. Proteins were wet-transferred using the Bio-Rad Trans-Blot Cell system (Bio-Rad Laboratories, United Kingdom) for 1 hour at 4˚C. The membrane was blocked with TBS-T (50

mM Tris-HCl, pH 7.6, 150 mM NaCl, 0.1% Tween 20) + 5% skimmed milk for 1 hour at room temperature before being incubated overnight at 4°C with rabbit anti-GFP or rabbit anti-RFP (both Abcam, 1 in 2000). The blot was then incubated with horseradish peroxidase–coupled anti-rabbit immunoglobulin (Dako, 1 in 2000) and subsequently visualised following 5 min incubation with enhanced chemiluminescence detection reagents ECL (EMD Millipore, United Kingdom), using the BioSpectrum Imaging System (Ultra-Violet Products Ltd). β-tubulin or b-catenin (Abcam, 1 in 1000) were used as house-keeping controls. Data were expressed as protein expression normalized to the control.

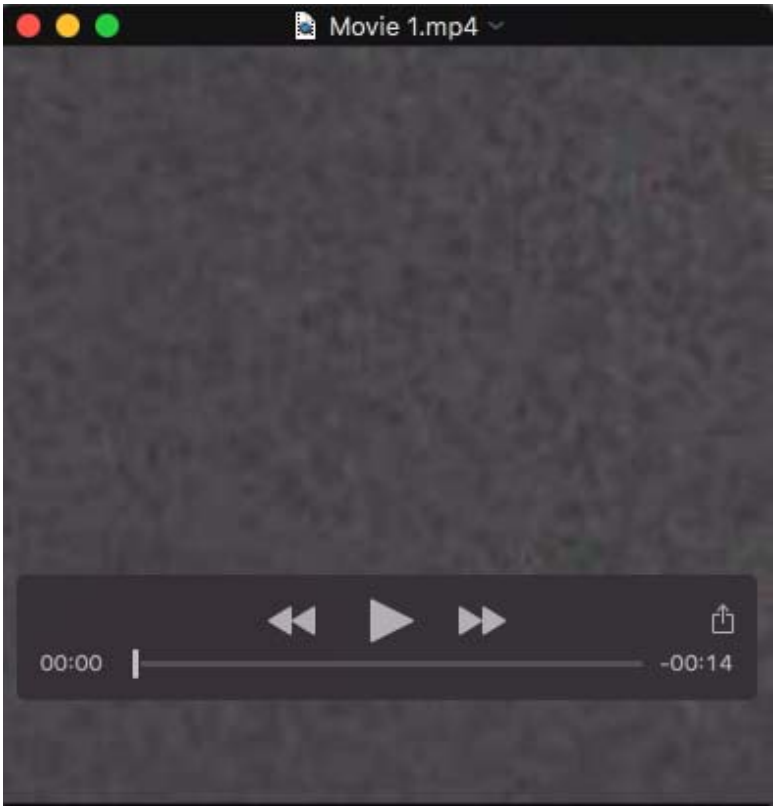

Movie 1. GCaMP6 fluorescence changes in E5 hindbrain.

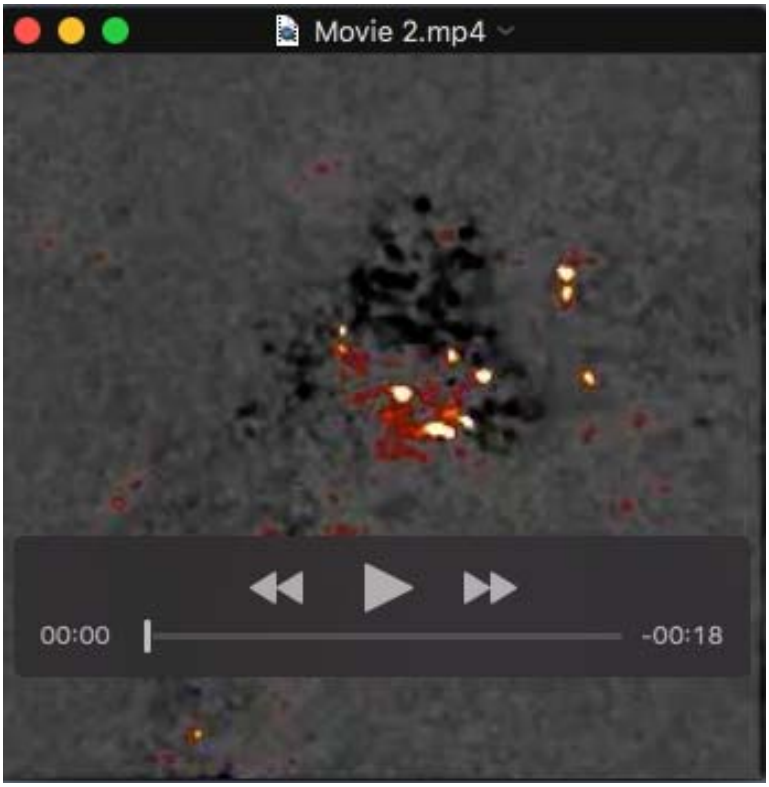

Movie 2. GCaMP6 fluorescence changes in E5 hindbrain.